Electronic annex to:

# Characterizing cosmochemical materials with genetic affinities to the Earth: Genetic and chronological diversity within the IAB iron meteorite complex

Authors: Emily A. Worsham, Katherine R. Bermingham, and Richard J. Walker

## 1. Samples

The samples analyzed are listed with their U.S. National Museum numbers (USNM #), where applicable in **Table S1**. Details regarding the methods used for cosmic ray exposure corrections and chemistry are also specified.

## 2. Analytical methods and data reduction

Iron meteorite pieces used for Mo and W analyses were digested in 30-40 ml of 8M HCl in *Savillex Teflon*® beakers which were heated at 130-140 °C on a hotplate for at least 48 hours. Silicate samples used for Mo isotope analyses were powdered in an agate mortar and pestle, and digested in 30 ml of a concentrated HF:$HNO_3$ mixture in 5:1 proportions on a hotplate at 130 °C. Samples for Os isotopic analyses were digested in *Pyrex*® Carius tubes using 2:1 concentrated $HNO_3$:HCl.

**Table S1.** List of iron meteorites studied here together with their USNM #. The analyses conducted for Os, Mo, and W isotopic compositions for each meteorite are marked with an "x". Also included are the methods used for CRE correction for Mo and W for each meteorite/group, and details about the chemistry for Mo and Os.

| Sample | USNM # | Os | Mo | W | Mo CRE corr.[a] | W CRE corr. | Mo from W chem.[b] | Os aliquoted/ adjacent[c] |
|---|---|---|---|---|---|---|---|---|
| **MG** | | | | | | | | |
| Canyon Diablo | 1530 | x | - | x | - | Not corrected | | adjacent |
| Landes | 5663 | x | x | x | sLL-sLM avg. slope | MG slope | yes | adjacent |
| Campo del Cielo | 5615 | x | x | x | Not corrected | Not corrected | yes | adjacent |
| Morasko | 6915 | x | x | x | sLL-sLM avg. slope | MG slope | no | both |
| Hope | 3477 | x | x | - | sLL-sLM avg. slope | - | no | aliquot |
| Bogou | 2245 | x | - | - | - | - | | adjacent |
| *MG mean/intercept* | | | | | Mean of individuals | MG intercept | | |
| **sLL** | | | | | | | | |
| Toluca | 460 | x | x | x | sLL slope | sLL slope | 1 of 3 | both |
| Bischtübe | 2666 | x | x | x | sLL slope | sLL slope | no | aliquot |
| Deport | 2267 | x | x | x | sLL slope | sLL slope | 1 of 2 | both |
| Goose Lake | 1332 | - | - | x | - | Not corrected | | - |
| *sLL intercept* | | | | | sLL intercept | sLL intercept | | |
| **sLM** | | | | | | | | |
| Edmonton (KY) | 1413 | x | x | x | sLM slope | sLM slope | no | aliquot |
| Maltahöhe | 6482 | x | x | x | sLM slope | sLM slope | no | aliquot |
| Persimmon Creek | 318 | x | x | x | Not corrected | Not corrected | yes | adjacent |
| *sLM intercept* | | | | | sLM intercept | sLM intercept | | |
| **sLH** | | | | | | | | |
| Tazewell | 3089 | x | x | - | sLL-sLM avg. slope | - | no | adjacent |
| Dayton | 1592 | - | x | - | Not corrected | - | no | - |
| Freda | 1342 | - | x | - | Not corrected | - | no | - |
| *sLH mean* | | | | | Mean of individuals | | | |
| **sHH** | | | | | | | | |
| ALHA80104 | | x | x | x | Not corrected | Not corrected | yes | adjacent |
| Kofa | 7009 | - | x | x | Not corrected | Not corrected | no | aliquot |
| Mount Magnet | 1746 | - | x | - | Not corrected | - | no | - |
| *sHH mean* | | | | | Mean of individuals | Not reported (n < 3) | | |
| **sHL** | | | | | | | | |
| Quarat al Hanish | 6176 | x | x | x | Not corrected | Not corrected | no | aliquot |
| Chebankol | 1731 | x | x | x | sLL-sLM avg. slope | MG-sLL-sLM avg. slope | no | aliquot |
| *sHL mean* | | | | | Mean of individuals | Not reported (n < 3) | | |
| Sombrerete | 5870 | x | x | x | sLL-sLM avg. slope | MG-sLL-sLM avg. slope | yes | adjacent |
| **Primitive achondrites** | | | | | | | | |
| Winona (Win) | 854 | - | x | - | Not corrected | - | no | - |
| HAH 193 (Win) | | - | x | - | Not corrected | - | no | - |
| NWA 725 | | - | x | - | Not corrected | - | no | - |
| GRA 95209 | | - | x | - | Not corrected | - | no | - |

*continued*

**Table S1.** Continued.

| Sample | | Os | Mo | W | Mo CRE corr.[a] | W CRE corr. | Mo from W chemistry[b] | Os aliquoted/ adjacent[c] |
|---|---|---|---|---|---|---|---|---|
| **Magmatic groups** | | | | | | | | |
| **IVB** | | | | | | | | |
| Skookum | 536 | x | x | - | IVB slope | - | no | aliquot |
| Hoba | 6506 | x | x | - | IVB slope | - | no | aliquot |
| Tlacotepec | 872 | x | x | - | IVB slope | - | no | aliquot |
| *IVB mean* | | | | | IVB intercept | | | |
| **IC** | | | | | | | | |
| Bendego | | x | x | - | sLL-sLM avg. slope | - | no | - |
| **IVA** | | | | | | | | |
| Maria Elena | 1221 | x | x | - | sLL-sLM avg. slope | - | no | aliquot |
| Yanhuitlan | 459 | x | x | - | sLL-sLM avg. slope | - | no | aliquot |
| Charlotte | 577 | x | x | - | Not corrected | - | no | aliquot |
| *IVA mean* | | | | | Mean of individuals | | | |
| **IIIAB** | | | | | | | | |
| Tamarugal | 6680 | x | x | - | sLL-sLM avg. slope | - | no | aliquot |
| Trenton | 2173 | x | x | - | sLL-sLM avg. slope | - | no | aliquot |
| Casas Grandes | 369 | x | x | - | sLL-sLM avg. slope | - | no | aliquot |
| *IIIAB mean* | | | | | Mean of individuals | | | |
| **Ungrouped iron meteorites** | | x | | | | | | |
| Chinga | 3451 | x | x | - | sLL-sLM avg. slope | - | no | aliquot |
| Tishomingo | 5862 | x | x | - | sLL-sLM avg. slope | - | no | aliquot |
| Dronino | 7203 | x | x | - | sLL-sLM avg. slope | - | no | aliquot |
| **Chondrites** | | | | | | | | |
| Richardton metal (H5) | | - | x | - | Not corrected | - | no | - |
| Allegan (H5) | 217 | - | x | - | Not corrected | - | no | - |
| St. Sauveur (EH5) | 7213 | - | x | - | Not corrected | - | no | - |

[a]For individual meteorites corrected using the slope-based, individual pre-exposure method, the slope used to calculate the pre-exposure value is given. Subgroups corrected using the intercept-derived, pre-exposure group method are denoted by "sLL intercept", for example. Subgroups or groups not corrected in this way are denoted by "MG mean of individuals", for example.

[b]Some Mo used for isotopic analyses was obtained as a byproduct of the W chemistry. These are labeled with "yes", or the number of analyses using Mo from the W chemistry conducted out of the total number of analyses.

[c]Osmium isotope data were obtained from either adjacent iron meteorite pieces to those used for Mo and W analyses, from aliquots from the digestion used for Mo or W analyses, or from both.

Analytical procedures for Os separation from iron meteorites were similar to those reported by Cook et al. (2004) and Walker (2012), and included solvent extraction and microdistillation. Purified samples were dissolved in ~1 µl concentrated HBr and 70-100 ng of Os were loaded onto an outgassed Pt filament. The sample was dried by applying a 0.5 A current to the filament. Once dry, ~0.5-0.8 µl of a saturated solution of $Ba(OH)_2$ was deposited on top of the sample and used as an electron emitter. For samples and standards, the Os isotope beams were collected in multiple Faraday cups using a static analytical routine (Walker, 2012). Osmium was measured as $OsO_3^-$, so the data were corrected for isobaric interferences from species which incorporate the heavy oxygen isotopes using the oxygen isotopic composition reported by Nier (1950) (e.g., Heumann et al., 1995). Possible isobaric interferences from Pt, Re, and W were monitored during each analyses at masses $^{198}Pt$, $^{183}W$, and $^{185}Re$ using a secondary electron multiplier detector. The intensities of the signals measured on these masses were typically < 2 mV, < 0.001 mV, and < 0.001 mV, respectively. Oxide corrections incorporated the contributions from these interferences. Interference and oxide corrections and mass-fractionation corrections for Os, Mo and W were done off-line.

Molybdenum separation and purification was achieved using a 2-stage anion exchange chromatographic procedure, and was analyzed using a double filament assembly (Worsham et al., 2016b). Between 500-1000 ng of Mo was loaded onto an outgassed Re evaporation filament in 6M HCl and dried at 0.6 A. For samples, once the deposit was dried, the current was increased slowly to ~2 A until a faint red glow was observed or until the sample transitioned from cloudy white to a colorless or bronze-colored deposit with a black rim. Two µl of a 5 µg/µl $La(NO_3)_3$ solution in 1M $HNO_3$ were then added as an electron emitter. The $La(NO_3)_3$ activator was partially dried at 0.6 A, then the current was increased to ~2 A until the solution was observed to

boil to dryness. Two µl of the $La(NO_3)_3$ solution were also added to the ionization filament, using the same drying procedure.

Molybdenum was measured as $^{x}MoO_3^-$ in a static, single-line measurement routine. Faraday cup detectors were electronically connected to amplifiers equipped with $10^{11}$ Ω resistors to collect the $^{x}Mo^{16}O_3^-$ beams, and a $10^{12}$ Ω resistor to measure the small $^{100}Mo^{18}O^{16}O_2^-$ beam, which was used for an *in-situ* oxide correction. This measurement allowed corrections for changes in the oxygen isotopic composition within and between analyses. During analyses, the amplifiers equipped with $10^{11}$ Ω resistors were electronically rotated to mitigate amplifier biases.

Tungsten was separated and purified from the sample matrix using a 4-stage cation and anion chromatographic procedure (Touboul and Walker, 2012). Prior to separation, an ether extraction step, using diisopropyl ether, was done to aid in the removal of the Fe matrix (Dodson et al., 1936). For W isotope analyses, methods from both Touboul and Walker (2012) and Archer et al. (2017) were used. Between 300-1000 ng of W was loaded onto outgassed Re ribbon and dried at 0.6-0.8 A. Both narrow (0.51 mm x 0.025 mm) and wide (0.76 mm x 0.030 mm) Re ribbon were used in this study. Thermal ionization of W from Re ribbon results in mV- to V-level Re signals. Using wide Re ribbon had a marginally higher sensitivity than when narrow ribbon was used; however, narrow ribbon was used for the majority of analyses to reduce the intensity of the Re signals, which can adversely affect the quality of the analysis. Wide ribbon was used when < 500 ng of sample was available. During sample loading, the current applied to the filament was increased until the filament glowed to a dull red for both samples and standards. A La and Gd (5 µg of each) mixed solution was used as an electron emitter. Tungsten was analyzed with nine Faraday cup detectors in a routine employing two static lines, which also monitored the Re signals.

Both analytical methods for analysis of W used in this study required a first-order oxide correction to correct for isobaric $^{17}O$- and $^{18}O$-bearing trioxide interferences, before the different secondary oxide corrections could be made (Touboul and Walker, 2012; Archer et al., 2017). For the first-order oxide correction in both methods, the $^{18}O/^{16}O$ ratio measured by Archer et al. (2017) was used in place of the Nier (1950) value used by Touboul and Walker (2012). This was done so that the data which were collected and corrected using both methods were consistent.

## 3. Neutron fluence dosimetry and cosmic ray exposure correction

A number of elements exhibit isotopic modifications as a result of CRE, including Os, Pt, Mo, and W. Osmium and Pt can be used as CRE dosimeters because neither shows nucleosynthetic variation at the bulk meteorite scale, but are strongly affected by CRE (e.g., Wittig et al., 2013). Osmium is used here.

Osmium isotopic data of IAB and magmatic iron meteorites are given in **Tables 1** and **S2**, respectively. The $\mu^{189}Os$ and $\mu^{190}Os$ isotope data are correlated, consistent with modification due to CRE. These data create an array which lies along a neutron production/burnout model calculated by Walker (2012) (**Fig. S1**). Osmium-189 and $^{190}Os$ are typically the most useful Os isotopes for use as neutron fluence dosimeters because they are major isotopes of Os and are characterized by comparatively large neutron capture cross sections and thermal resonance integrals (see Table 2 from Walker, 2012). For example, $^{189}Os$ has a resonance integral of 674 b. By comparison, the other Os isotopes have smaller resonance integrals (i.e. Os isotopes with > 1% abundance have 4.6 to 500 b resonance integrals; Mughabghab, 2003). Only low-abundance Os isotopes have higher neutron capture cross sections than $^{189}Os$ and $^{190}Os$.

**Table S2.** $\mu^{189}$Os and $\mu^{190}$Os values for some magmatic iron meteorites. The $\mu^{189}$Os data were used to correct the Mo isotopic compositions measured in these iron meteorites (**Table S3** and **S7**).

| Sample | n | $\mu^{189}$Os | 2SD | $\mu^{190}$Os | 2SD |
|---|---|---|---|---|---|
| **Magmatic iron meteorites** | | | | | |
| **IVB** | | | | | |
| Skookum | 1 | -16 | 5 | 6 | 6 |
| Hoba | 1 | -6 | 5 | 2 | 6 |
| Tlacotepec | 1 | -60 | 5 | 37 | 6 |
| **IC** | | | | | |
| Bendego | 1 | -40 | 6 | 17 | 4 |
| **IVA** | | | | | |
| Maria Elena | 1 | -39 | 5 | 10 | 6 |
| Yanhuitlan[a] | | -22 | 12 | 10 | 13 |
| Charlotte | 1 | 3 | 6 | 2 | 6 |
| **IIIAB** | | | | | |
| Tamarugal[a] | | -16 | 12 | 11 | 12 |
| Trenton | 1 | -17 | 5 | 12 | 5 |
| Casas Grandes | 1 | -34 | 5 | 13 | 5 |
| **Ungrouped iron meteorites** | | | | | |
| Chinga | 1 | -5 | 5 | -3 | 6 |
| Tishomingo | 1 | -12 | 5 | 4 | 6 |
| Dronino | 1 | -16 | 5 | 8 | 6 |

[a]Data are from Walker (2012).

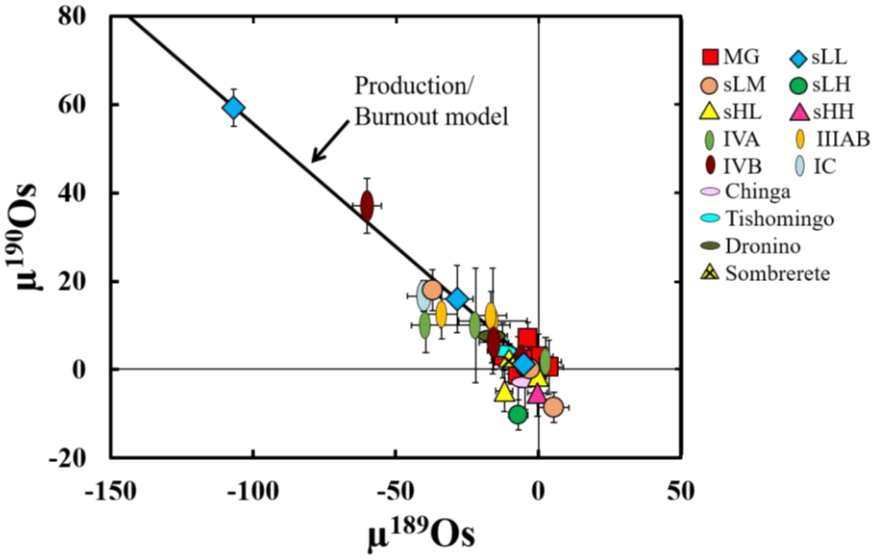


**Fig. S1.** $\mu^{189}$Os vs. $\mu^{190}$Os for IAB, magmatic, and ungrouped iron meteorites. Osmium isotope production/burnout, due to neutron capture on isotopes of Os, Re, Ir, and W, was calculated by Walker (2012), and is shown for reference.

Molybdenum isotope data are correlated with the Os isotope data, indicating that Mo is also modified by CRE (**Fig. 1**). Because $^{95}$Mo has the largest neutron capture cross section and resonance integral of the Mo isotopes by a wide margin (Mughabghab, 2003), the most significant nuclear reaction affecting the Mo isotopic compositions used in this study is likely: $^{95}$Mo(n,$\gamma$)$^{96}$Mo. Molybdenum-96 is used in the normalizing ratio, so all Mo isotope ratios may potentially be modified by high neutron fluence conditions. When the Mo data were normalized to $^{96}$Mo, the correlations of each Mo isotope with $\mu^{189}$Os were used to correct for CRE effects (**Table 2**). Tungsten isotopic compositions were also corrected for CRE (**Table 3**). Measured Mo and W isotopic compositions which are not CRE-corrected are given in **Tables S3** and **S4**.

Corrections for CRE modification of the W and Mo isotopic compositions were done two different ways in this study, depending on the precision of the $\mu^{189}$Os vs. $\mu^{i}$Mo or $\mu^{182}$W linear correlation for a given group or subgroup (**Tables S1, S5-S6)**. The intercept-derived, group pre-exposure method of correction, in which the intercept of the of $\mu^{189}$Os vs. $\mu^{i}$Mo or $\mu^{182}$W correlation is taken as the pre-exposure $\mu^{i}$Mo or $\mu^{182}$W value, is used for subgroups which define precise correlations on plots of $\mu^{189}$Os vs. $\mu^{i}$Mo or $\mu^{182}$W, determined by linear regression (using ISOPLOT – Ludwig, 2003). The precisions of the slopes and intercepts vary among meteorite subgroups, due to the uncertainties of the measurements and the magnitude of the CRE effects.

For Mo isotopes, the most precise correlations were obtained for the sLL and sLM subgroups (and the IVB magmatic group). For $\mu^{182}$W, the most precise correlations were obtained for the MG and the sLL and sLM subgroups. For these subgroups, slopes and intercepts of the regressions of $\mu^{189}$Os vs. $\mu^{i}$Mo are reported in **Table S5**, and those of $\mu^{189}$Os vs. $\mu^{182}$W are reported in **Table S6**. These subgroups are denoted in **Table S1** as being corrected using the intercept-derived, group pre-exposure method.

**Table S3.** Molybdenum isotopic compositions for IAB complex iron meteorites and other meteorites. Data are uncorrected for CRE effects.

| Sample | n[a] | $\mu^{92}$Mo | ± | $\mu^{94}$Mo | ± | $\mu^{95}$Mo | ± | $\mu^{97}$Mo | ± | $\mu^{100}$Mo | ± |
|---|---|---|---|---|---|---|---|---|---|---|---|
| **MG** | | | | | | | | | | | |
| Landes | 1 | -41 | 92 | -12 | 29 | -15 | 14 | -1.4 | 4.8 | 1 | 34 |
| Campo del Cielo | 1 | -28 | 92 | 0 | 29 | -8 | 14 | 0.4 | 4.8 | -4 | 34 |
| Morasko | 1 | -22 | 71 | -5 | 21 | -14 | 9 | -4.1 | 4.7 | -5 | 31 |
| Hope | 1 | 7 | 68 | 7 | 24 | -5 | 16 | -0.1 | 4.7 | 11 | 30 |
| *MG mean* | | -21 | 21 | -2 | 8 | -10 | 5 | -1.3 | 2.0 | 1 | 7 |
| **sLL** | | | | | | | | | | | |
| Toluca | 3 | 9 | 45 | 10 | 17 | -6 | 6 | 1.1 | 2.0 | 1 | 3 |
| Bischtübe | 1 | -65 | 90 | -18 | 28 | -25 | 15 | -3.9 | 6.0 | -3 | 24 |
| Deport | 2 | -110 | 49 | -50 | 14 | -58 | 2 | -7.5 | 7.0 | -2 | 28 |
| *sLL mean* | | -55 | 120 | -19 | 60 | -30 | 52 | -3.4 | 8.6 | -1 | 5 |
| **sLM** | | | | | | | | | | | |
| Edmonton (KY) | 2 | -31 | 110 | 0 | 36 | -12 | 17 | 3.0 | 5.2 | -3 | 33 |
| Maltahöhe | 1 | -48 | 71 | -16 | 21 | -24 | 9 | -5.1 | 4.7 | -1 | 31 |
| Persimmon Creek | 1 | 18 | 92 | 17 | 29 | 2 | 14 | 1.7 | 4.8 | 1 | 34 |
| *sLM mean* | | -20 | 68 | 0 | 33 | -11 | 27 | -0.2 | 8.7 | -1 | 4 |
| **sLH** | | | | | | | | | | | |
| Tazewell | 1 | -64 | 71 | -11 | 21 | -18 | 9 | -2.8 | 4.7 | -8 | 31 |
| Dayton | 1 | 19 | 71 | 14 | 21 | -1.1 | 9 | -3.7 | 4.7 | -1 | 31 |
| Freda | 1 | -58 | 68 | -16 | 24 | -17 | 16 | 0.3 | 4.7 | -9 | 30 |
| *sLH mean* | | -34 | 93 | -5 | 32 | -12 | 19 | -2.1 | 4.2 | -6 | 9 |
| **sHH** | | | | | | | | | | | |
| ALHA80104 | 2 | 44 | 92 | 77 | 29 | 28 | 14 | 26 | 5 | 4.6 | 34 |
| Kofa | 1 | 8 | 71 | 52 | 21 | 20 | 8.6 | 23 | 5 | 2.7 | 31 |
| Mount Magnet | 1 | 173 | 68 | 120 | 24 | 54 | 16 | 24 | 5 | 42 | 30 |
| *sHH mean* | | 75 | 173 | 83 | 69 | 34 | 36 | 24 | 3 | 16 | 44 |
| **sHL** | | | | | | | | | | | |
| Quarat al Hanish | 1 | 88 | 71 | 95 | 21 | 37 | 8.6 | 20 | 5 | 30 | 31 |
| Chebankol | 1 | 152 | 71 | 117 | 21 | 47 | 8.6 | 25 | 5 | 40 | 31 |
| *sHL mean* | | 120 | 90 | 106 | 32 | 42 | 13 | 23 | 6 | 35 | 14 |
| Sombrerete | 1 | 206 | 92 | 166 | 29 | 109 | 14 | 55 | 5 | 72 | 34 |
| **Primitive achondrites** | | | | | | | | | | | |
| Winona (Win) | 1 | 20 | 90 | 18 | 30 | 5 | 15 | -1.3 | 3.3 | 1 | 22 |
| HAH 193 (Win) | 1 | 40 | 90 | 25 | 30 | 8 | 15 | 4.9 | 3.3 | 5 | 22 |
| NWA 725 | 1 | 155 | 68 | 120 | 24 | 52 | 16 | 30 | 5 | 63 | 30 |
| GRA 95209 (Lod) | 1 | 148 | 90 | 110 | 30 | 48 | 15 | 21 | 3 | 24 | 22 |
| **IVB** | | | | | | | | | | | |
| Skookum | 4 | 248 | 70 | 157 | 23 | 109 | 8.6 | 54 | 3 | 100 | 25 |
| Hoba | 2 | 186 | 117 | 136 | 28 | 105 | 15 | 56 | 8 | 67 | 30 |
| Tlacotepec | 3 | 162 | 50 | 115 | 13 | 73 | 2.9 | 46 | 2 | 85 | 30 |
| *IVB mean* | | 199 | 89 | 136 | 43 | 96 | 39 | 52 | 10 | 84 | 33 |
| **IC** | | | | | | | | | | | |
| Bendego | 1 | 124 | 90 | 91 | 28 | 28 | 15 | 21 | 6 | 37 | 24 |
| **IVA** | | | | | | | | | | | |
| Maria Elena | 1 | 62 | 92 | 69 | 29 | 24 | 14 | 14 | 5 | 11 | 34 |
| Yanhuitlan | 1 | 38 | 92 | 54 | 29 | 21 | 14 | 21 | 5 | 20 | 34 |
| Charlotte | 1 | 137 | 110 | 87 | 36 | 38 | 17 | 17 | 5 | 40 | 33 |
| *IVA mean* | | 79 | 103 | 70 | 33 | 27 | 19 | 17 | 7 | 24 | 30 |
| **IIIAB** | | | | | | | | | | | |
| Tamarugal | 3 | 114 | 31 | 100 | 14 | 38 | 8 | 22 | 11 | 33 | 16 |
| Trenton | 1 | 90 | 68 | 87 | 24 | 29 | 16 | 21 | 5 | 43 | 30 |
| Casas Grandes | 1 | 140 | 110 | 102 | 36 | 35 | 17 | 23 | 5 | 57 | 33 |
| *IIIAB mean* | | 115 | 49 | 96 | 17 | 34 | 9.4 | 22 | 2 | 44 | 24 |
| **Ungrouped iron meteorites** | | | | | | | | | | | |
| Chinga | 2 | 226 | 148 | 163 | 46 | 112 | 14 | 54 | 4 | 77 | 56 |
| Tishomingo | 2 | 201 | 93 | 141 | 22 | 93 | 13 | 46 | 5 | 75 | 49 |
| Dronino | 1 | 142 | 90 | 129 | 28 | 89 | 15 | 52 | 6 | 63 | 24 |
| **Chondrites** | | | | | | | | | | | |
| Richardton metal (H5) | 1 | 100 | 92 | 105 | 29 | 53 | 14 | 30 | 5 | 11 | 34 |
| Allegan (H5) | 1 | 43 | 110 | 52 | 36 | 22 | 17 | 19 | 5 | 21 | 33 |
| St. Sauveur (EH5) | 1 | 103 | 110 | 59 | 36 | 25 | 17 | 11 | 5 | 42 | 33 |

**Table S4.** Tungsten isotopic compositions for IAB complex iron meteorites. Data are uncorrected for CRE effects.

| Sample | Method | n | $\mu^{182}W_{186/183}$ | ± | $\mu^{182}W_{186/184}$ | ± | $\mu^{183}W$ | ± | $\Delta t_{CAI}$ | ± |
|---|---|---|---|---|---|---|---|---|---|---|
| **MG** | | | | | | | | | | |
| Canyon Diablo | I | 1 | -312 | 7 | -311 | 9 | | | 3.4 | 0.7 |
| Landes | I | 1 | -322 | 5 | -322 | 6 | | | 2.4 | 0.4 |
| Campo del Cielo | I | 1 | -305 | 5 | -305 | 6 | | | 4.2 | 0.5 |
| Morasko | II | 1 | -332 | 4 | -335 | 6 | -7 | 7 | 1.5 | 0.3 |
| *MG intercept* | | | -312 | 6 | | | | | 3.4 | 0.7 |
| **sLL** | | | | | | | | | | |
| Toluca | I | 2 | -302 | 5 | -301 | 6 | | | 4.6 | 0.5 |
| Bischtübe | II | 1 | -345 | 4 | -355 | 6 | -14 | 7 | 0.3 | 0.3 |
| Deport | I, II | 2 | -457 | 11 | -460 | 6 | -9 | 7 | -6.7 | 0.5 |
| Goose Lake | I | 1 | -298 | 6 | -303 | 8 | | | 4.9 | 0.8 |
| *sLL intercept* | | | -297 | 8 | | | | | 5.0 | 1.0 |
| **sLM** | | | | | | | | | | |
| Edmonton (KY) | II | 1 | -304 | 4 | -308 | 6 | -6 | 7 | 4.3 | 0.4 |
| Maltahöhe | II | 1 | -340 | 4 | -342 | 6 | -4 | 7 | 0.8 | 0.3 |
| Persimmon Creek | I | 1 | -287 | 5 | -288 | 6 | | | 6.3 | 0.7 |
| *sLM intercept* | | | -297 | 5 | | | | | 5.1 | 0.6 |
| **sHH** | | | | | | | | | | |
| ALHA80104 | I | 1 | -345 | 5 | -345 | 6 | | | 0.3 | 0.4 |
| Kofa | II | 1 | -330 | 5 | -335 | 7 | -8 | 7 | 1.6 | 0.5 |
| **sHL** | | | | | | | | | | |
| Quarat al Hanish | II | 1 | -335 | 4 | -331 | 7 | 2 | 7 | 1.2 | 0.4 |
| Chebankol | II | 1 | -345 | 4 | -344 | 6 | 2 | 7 | 0.4 | 0.3 |
| Sombrerete | I | 2 | -331 | 5 | -330 | 6 | | | 1.6 | 0.4 |

The slope-derived, individual pre-exposure Mo or W isotopic composition of an individual meteorite is obtained by projecting the $\mu^{i}$Mo or $\mu^{182}$W value of a sample with a given $\mu^{189}$Os to a $\mu^{189}$Os of zero. This correction utilizes the simple linear equation and well-defined slopes of correlations between $\mu^{189}$Os vs. $\mu^{i}$Mo or $\mu^{182}$W.

The Mo and $^{182}$W isotopic compositions of individual meteorites within the sLL and sLM subgroups (and the MG for $^{182}$W) were corrected using the respective slopes of their subgroups. For Mo, other IAB and magmatic meteorites for which CRE-correction was necessary were corrected using the average of the sLL and sLM slopes. For $^{182}$W, IAB meteorites for which correction was necessary were corrected using the average slope of the MG, sLL, and sLM

subgroups. For individual meteorites corrected using an average slope, the 2SD of the slopes used to calculate the average was incorporated into the uncertainties of the data.

Of note, the W isotopic composition can be significantly affected by CRE (more so than Mo). Thus, the $\mu^{182}W$ values that are calculated for each individual meteorite using the slope of the $\mu^{189}Os$ vs. $\mu^{182}W$ correlation results in more uncertain pre-exposure values than those resulting from using the intercept-derived, group pre-exposure correction method (**Table S1, Table 3**). This is because the uncertainty of the slope is propagated through the calculation of the $\mu^{182}W$ value for an individual meteorite, and the larger the CRE effect, the larger the propagated uncertainty. This results in the $\mu^{182}W$ values that overlap within uncertainties for individual MG, sLM, and sLL meteorites. Therefore, the intercept-derived, group pre-exposure $\mu^{182}W$ is the best number by which to compare and contrast the pre-exposure $\mu^{182}W$ for each group.

The isotopic compositions of several meteorites were not corrected for CRE using the slope-derived, individual correction method (see **Table S1, Tables 2-3)** because they were minimally affected by CRE ($\mu^{189}Os$ values > -1; e.g., Campo del Cielo, Persimmon Creek, ALHA 80104). Osmium data were not collected due to low Os concentrations for four samples: Dayton, Freda, Kofa, and Mount Magnet. Possible uncorrected CRE effects on these meteorites do not affect the interpretations of the Mo and W isotopic data, as discussed in Section 4.2 of the main text. Osmium data were also not obtained for primitive achondrites or chondrites, because stony meteorites generally have much lower exposure ages than iron meteorites.

**Table S5**. Linear regression results of the measured $\mu^{189}$Os vs. $\mu^{i}$Mo for the sLL and sLM subgroups and IVB magmatic iron meteorite group using data from **Tables 1** and **S2-S3,** calculated using ISOPLOT. The MG is not included because it does not produce well-defined correlations due to the limited range of CRE effects in MG irons studied here. The mean square weighted deviation (MSWD) is a measure of scatter about the regression.

| | **n** | **Slope** | **±** | **Intercept** | **±** | **MSWD** |
|---|---|---|---|---|---|---|
| **sLL** | 3 | | | | | |
| 92 | | 1.12 | 0.63 | 7 | 44 | 0.91 |
| 94 | | 0.57 | 0.21 | 10 | 16 | 0.84 |
| 95 | | 0.50 | 0.06 | -4.8 | 6.3 | 0.75 |
| 97 | | 0.090 | 0.069 | 1.3 | 2.1 | 0.90 |
| 100 | | 0.050 | 0.27 | 1.6 | 3.3 | 0.11 |
| **sLM** | 3 | | | | | |
| 92 | | 1.3 | 2.5 | -3 | 66 | 0.29 |
| 94 | | 0.69 | 0.77 | 9 | 21 | 0.24 |
| 95 | | 0.56 | 0.35 | -3.9 | 10 | 0.73 |
| 97 | | 0.18 | 0.15 | 1.9 | 3.4 | 0.64 |
| 100 | | 0.01 | 0.99 | -1 | 22 | 0.03 |
| **IVB** | 3 | | | | | |
| 92 | | 1.38 | 1.60 | 247 | 76 | 1.2 |
| 94 | | 0.66 | 0.45 | 155 | 22 | 2.4 |
| 95 | | 0.73 | 0.19 | 117 | 10 | 1.5 |
| 97 | | 0.179 | 0.068 | 57 | 3.4 | 0.01 |
| 100 | | -0.08 | 0.71 | 84 | 24 | 2.8 |
| **Average sLL and sLM slope** | | | | | | |
| 92 | | 1.21 | 0.25 | | | |
| 94 | | 0.63 | 0.17 | | | |
| 95 | | 0.53 | 0.09 | | | |
| 97 | | 0.14 | 0.13 | | | |
| 100 | | 0.03 | 0.06 | | | |

**Table S6**. Linear regressions of the measured $\mu^{189}$Os vs. $\mu^{182}$W for each subgroup for which > 2 samples were measured using data from **Tables 1** and **S4**. The intercept gives the pre-exposure $\mu^{182}$W for each subgroup.

| | **n** | **Slope** | **±** | **Intercept** | **±** | **MSWD** |
|---|---|---|---|---|---|---|
| MG | 4 | 1.67 | 0.76 | -312 | 6 | 0.1 |
| sLL slope | 3 | 1.52 | 0.14 | -297 | 8 | 1.6 |
| sLM slope | 3 | 1.18 | 0.20 | -297 | 5 | 1.8 |
| Average slope | | 1.46 | 0.50 | | | |

For some samples it may be important to account for the Re/Os ratio (Qin et al., 2015). This is because the neutron capture effects on Re isotopes may affect the Os isotopic composition (Qin et al., 2015). The equations used to calculate pre-exposure $\mu^{182}W$ values for individual meteorites from Qin et al. (2015) were derived using data from Carbo (IID) and utilize the measured Re/Os concentration ratio and the measured Os isotopic composition (e.g., $\mu^{189}Os$) in a given meteorite. When this was done using Re/Os data from Worsham et al. (2016a) for individual meteorites in this study, the corrected $\mu^{182}W$ values were more negative than those reported in the main text. This is likely because the $\mu^{189}Os$ vs. $\mu^{182}W$ slope used to derive the equations in Qin et al (2015) was more shallow than some of the slopes reported here (e.g., 1.27 ± 0.19 from that study vs. the sLM slope of 1.18 ± 0.20, the sLL slope of 1.52 ± 0.14, and the MG slope of 1.67 ± 0.76). For example, Deport (sLL), is under-corrected using the equations of Qin et al. (2015), resulting in inconsistent pre-exposure $\mu^{182}W$ values for some samples from the same group. Further, because the group pre-exposure $\mu^{182}W$ values for the MG, sLL, and sLM subgroups are calculated using linear regressions internal to each subgroup, minor differences in the $\mu^{189}Os$ vs. $\mu^{182}W$ slopes caused by variations in Re/Os are likely largely accounted for. When the correction method of Qin et al. (2015) was used for Chebankol and Sombrerete, which required individual CRE correction, the pre-exposure $\mu^{182}W$ value of Chebankol was -332, and that of Sombrerete was -319. The pre-exposure value calculated for Chebankol when accounting for Re/Os is in better agreement with the other sHL iron, Quarat al Hanish, but this may also be due to the use of a shallower slope. Sombrerete is not significantly different. Because the CRE effects in Mo are relatively small, Re/Os variability likely has a negligible effect on the Mo CRE corrections.

## 4. Molybdenum isotope data

Cosmic ray exposure-corrected Mo isotopic compositions of the IAB meteorites, primitive achondrite, chondrites, and average magmatic iron meteorite groups are reported in **Table 2** and **Fig. S2**. The CRE-corrected Mo isotopic compositions of individual magmatic iron meteorites are reported in **Table S7**.

The classification of Hope and Morasko as MG irons was questioned by Pilski et al. (2013), due primarily to comparatively low Ir abundances. The consistency of the Mo isotopic compositions, however, indicates that Hope and Morasko are genetically associated with the MG. The low Ir abundances may be a result of fractional crystallization (Worsham et al., 2016a).

**Table S7.** CRE-corrected Mo isotopic compositions of magmatic iron meteorite groups

| Sample | n[a] | $\mu^{92}$Mo | ± | $\mu^{94}$Mo | ± | $\mu^{95}$Mo | ± | $\mu^{97}$Mo | ± | $\mu^{100}$Mo | ± |
|---|---|---|---|---|---|---|---|---|---|---|---|
| IC | | | | | | | | | | | |
| Bendego | 1 | 172 | 91 | 117 | 29 | 49 | 16 | 26 | 8 | 37 | 24 |
| IIIAB | | | | | | | | | | | |
| Tamarugal | 3 | 133 | 35 | 110 | 16 | 46 | 11 | 24 | 11 | 33 | 16 |
| Trenton | 1 | 110 | 68 | 97 | 24 | 37 | 16 | 23 | 5 | 43 | 30 |
| Casas Grandes | 1 | 181 | 111 | 123 | 37 | 53 | 17 | 27 | 7 | 57 | 33 |
| IVA | | | | | | | | | | | |
| Maria Elena | 1 | 109 | 93 | 94 | 30 | 44 | 15 | 19 | 7 | 11 | 34 |
| Yanhuitlan | 1 | 65 | 93 | 68 | 30 | 32 | 15 | 24 | 6 | 20 | 34 |
| Charlotte | 1 | 137 | 110 | 87 | 36 | 38 | 17 | 17 | 5 | 40 | 33 |
| IVB | | | | | | | | | | | |
| Skookum | 4 | 270 | 74 | 168 | 24 | 120 | 10 | 57 | 3 | 100 | 25 |
| Hoba | 2 | 195 | 117 | 140 | 28 | 109 | 15 | 57 | 8 | 67 | 30 |
| Tlacotepec | 3 | 245 | 109 | 154 | 30 | 117 | 12 | 57 | 4 | 85 | 30 |

[a]n is the number of analyses. Uncertainties are the 2SD of the standards or analyses ($n \leq 3$) or 2SE ($n > 3$).

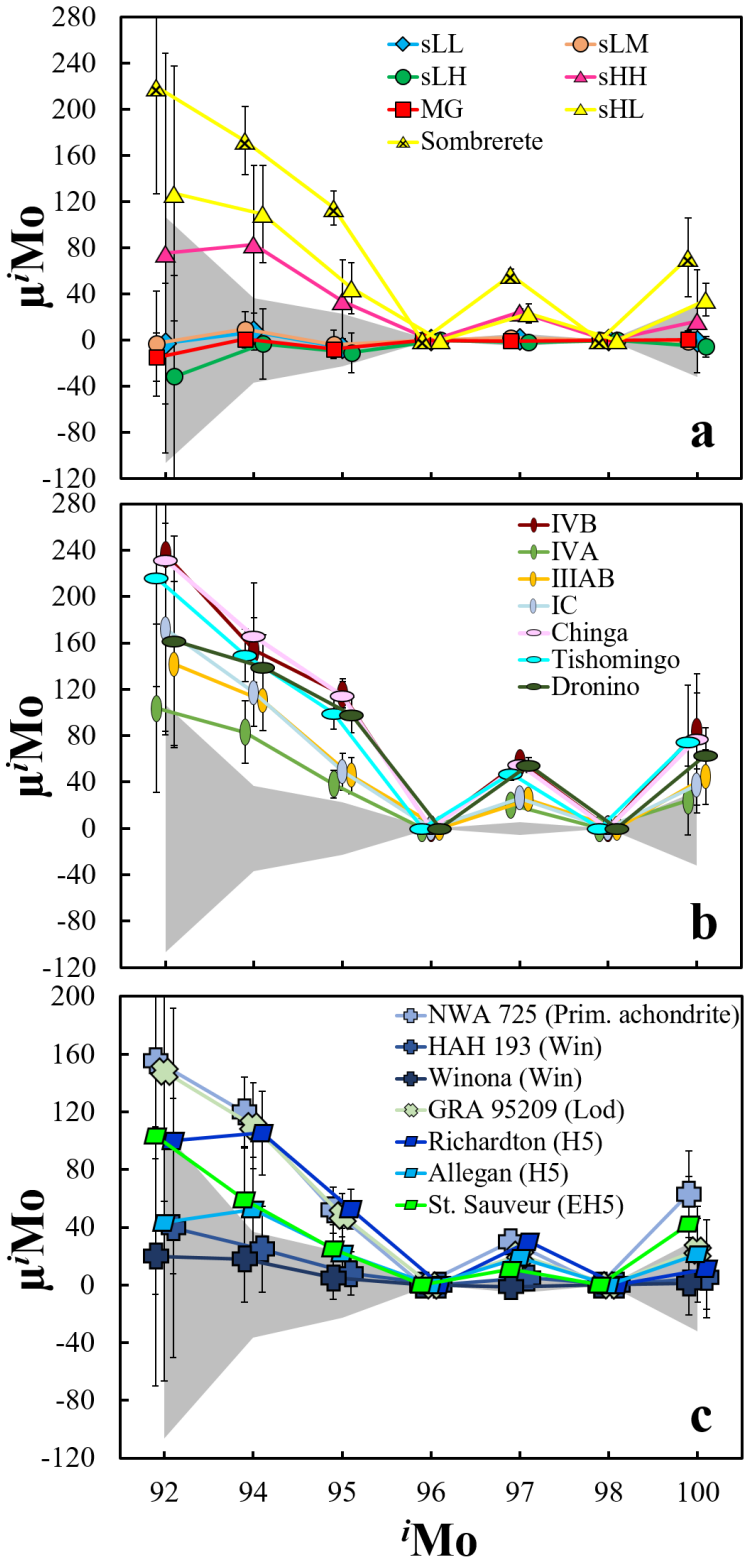


**Fig. S2.** $\mu^{i}$Mo for (a) IAB complex iron meteorites, (b) Magmatic iron meteorite groups and ungrouped irons, and (c) H5 ordinary and enstatite chondrites, winonaites (Win), lodranite GRA 95209 (Lod), and primitive achondrite NWA 725. Note the change of scale in (c).

## 5. Tungsten-183 data

Nucleosynthetic anomalies in $\mu^{183}W$ in IVB iron meteorites have been observed (Qin et al., 2008). Using the method of Touboul and Walker (2012), the $^{183}W/^{184}W$ ratio is used for the second-order correction to account for variable oxygen isotopic compositions within and between analyses, such that $\mu^{183}W$ cannot be measured using this method. The Archer et al. (2017) W analytical method allows for the *in situ* measurement of the O isotopic composition, so the $\mu^{183}W$ values can be measured precisely. The $\mu^{183}W$ results are presented in **Table S4**. No resolvable W nucleosynthetic effects are observed in the IAB meteorites which were analyzed using method of Archer et al. (2017). This indicates that nucleosynthetic variability cannot account for differences in the reported $\mu^{182}W$ values between the IAB subgroups.

## 6. IAB parent bodies, genetics, and chronology

### *6.1 Number of parent bodies represented in the IAB complex*

Molybdenum isotope data from this study and trace element abundance data from Wasson and Kallemeyn (2002) and Worsham et al. (2016a) were primarily used to reject genetic links between the IAB subgroups. These criteria and others are outlined in **Table S8**, which gives the primary evidence used to reject a genetic link (e.g., the $\mu^{97}Mo$ value) between pairs of subgroups (e.g., the MG and the sHL subgroup) for all subgroup pairs.

Typically, when a genetic link is rejected, the interpretation is that the two meteorites or meteorite groups originated on separate parent bodies. However, the implicit assumption is that each parent body is isotopically homogenous. Alternately, some or all of the IAB subgroups may

have originated on a single isotopically heterogeneous ruble pile parent body. This cannot be tested using the existing dataset, but it is considered unlikely. Some IAB meteorites may have originated on a large parent body (e.g., Rasmussen, 1989), where gravitational forces would likely preclude a rubble pile model. Further, temperatures on the IAB parent body or bodies were high enough to melt metal, and some winonaites and IAB silicates may have reached temperatures between 750-1200 ºC (e.g., Benedix et al., 2000). Under these conditions, isotopic equilibrium would likely be reached. Regardless, the Mo isotopic compositions indicate that the precursor materials of certain subgroups originated in separate isotopic reservoirs, whether they were consolidated into a single parent body or not.

**Table S8.** Evidence used to determine how IAB subgroups may be related. Table entries are labeled with the evidence which was used to reject a genetic link between different subgroups. Subgroup pairs for which all data support a genetic link are labeled "Common" for common parent body. The "Mo" and "W" entries specifically refer to the $\mu^{97}$Mo and $\mu^{182}$W isotopic compositions.

| | MG | sLL | sLM | sLH | sHL | sHH | Sombrerete | Winonaites |
|---|---|---|---|---|---|---|---|---|
| MG | - | | | | | | | |
| sLL | Common | - | | | | | | |
| sLM | HSE[a,b], Ni[b] | HSE[a,b], Ni[b] | - | | | | | |
| sLH | HSE[a,b], Ni[b] | HSE[a,b], Ni[b] | Common | - | | | | |
| sHL | Mo, W | Mo, W | Mo, W | Mo | - | | | |
| sHH | Mo, W | Mo, W | Mo, W | Mo | *W, HSE[a,b] | - | | |
| Sombrerete | Mo | Mo | Mo | Mo | Mo | Mo | - | |
| Winonaites | Common | Common | Mineralogy[c] | Mineralogy[c] | Mo | Mo | Mo | - |

[a]Highly siderophile element (HSE) data from Worsham et al. (2016a)
[b]Other HSE abundance data (i.e., Au) and Ni data from Wasson and Kallemeyn (2002)
[c]Mineralogical and major element abundance evidence from McCoy et al. (1993) and Benedix et al (2000)
*A genetic link between the sHL and sHH groups cannot be rejected, but W isotope data and HSE abundance data suggest these may have come from separate parent bodies (see Section 5.3).

*6.2. Two-stage Hf-W model ages*

Two-stage metal-silicate segregation model ages ($\Delta t_{CAI}$) are calculated using the equation:

$$\Delta t_{CAI} = \frac{1}{\lambda} ln\left(\frac{\mu^{182}W_{Sample} - \mu^{182}W_{Chondrite}}{\mu^{182}W_{CAI} - \mu^{182}W_{Chondrite}}\right)$$

where $\lambda$ is the $^{182}$Hf decay constant (0.078 ± 0.002; Vockenhuber et al., 2004), $\mu^{182}W_{Chondrite}$ is the present-day chondritic $\mu^{182}$W (-190 ± 10; Kleine et al., 2004), and $\mu^{182}W_{CAI}$ is the initial $\mu^{182}$W of CAIs (-349 ± 7; Kruijer et al., 2014). The chondritic $\mu^{182}$W of -190 assumes that the precursor materials had uniform $^{180}$Hf/$^{184}$W of 1.29 ± 0.09. The model age uncertainties reported here do not take into account the uncertainties associated with the $^{182}$Hf decay constant, the CAI initial ratio, or Hf/W in the precursor materials.

Given this equation, the relative model ages of the subgroups either represent differences in the timing of metal-silicate segregation among the subgroups, or more complex differentiation and/or mixing processes which incorporated precursor materials with different initial Hf/W, or reservoirs which evolved to different H/W ratios. For example, a single parent body may have been partially differentiated, yielding $\mu^{182}$W values in the segregated metal that are similar to those of magmatic iron meteorites. Subsequent mixing of the remaining W (e.g., from a catastrophic breakup and reassembly event; Benedix et al., 2000) from a reservoir, which evolved to a higher Hf/W ratio, could lead to less negative $\mu^{182}$W values. This would result in erroneously young metal-silicate segregation ages, and an interpretation invoking an external heat source as favored in the main text. Alternately, metal silicate segregation resulting from relatively late impact-induced melting would yield $\mu^{182}$W values which are less negative than those of magmatic iron meteorite groups. However, if the impactor was differentiated early,

mixing of W from the impactor's core with W in the newly segregated metal would lead to erroneously old metal-silicate segregation ages. These scenarios cannot be excluded at this time.

## References


Archer G. J., Mundl A., Walker R. J., Worsham E.A., and Bermingham K.R. (2017) High-precision analysis of $^{182}W/^{184}W$ and $^{183}W/^{184}W$ by negative thermal ionization mass spectrometry: Per-integration oxide corrections using measured $^{18}O/^{16}O$. *Int. J. Mass. Spectrom.* **414**, 80-86.

Benedix G. K., McCoy T. J., Keil K., and Love S. G. (2000) A petrologic study of the IAB iron meteorites: Constraints on the formation of the IAB-Winonaite parent body. *Meteorit. Planet. Sci.* **35,** 1127-1141.

Cook D. L., Walker R. J., Horan M. F., Wasson J. T., and Morgan J. W. (2004) Pt-Re-Os systematics of group IIAB and IIIAB iron meteorites. *Geochim. Cosmochim. Acta* **68**, 1413-1431.

Dodson R. W., Forney G. J., and Swift E. H. (1936) The extraction of ferric chloride from hydrochloric acid solutions by isopropyl ether. *J. Am. Chem. Soc.* **58**, 2573-2577.

Heumann K. G., Eisenhut S., Gallus S., Hebeda E. H., Nusko R., Vengosh A., and Walczyk T. (1995) Recent developments in thermal ionization mass spectrometric techniques for isotope analysis. *Analyst* **120**, 1291-1299.

Kleine T., Mezger K., Münker C., Palme H., Bischoff A. (2004) $^{182}Hf–^{182}W$ isotope systematics of chondrites, eucrites, and Martian meteorites: Chronology of core formation and mantle differentiation in Vesta and Mars, *Geochim. Cosmochim. Acta* **68**, 2935–2946.

Kruijer T. S., Kleine T., Fischer-Gödde M., Burkhardt C., and Wieler R. (2014) Nucleosynthetic W isotope anomalies and the Hf-W chronometry of Ca–Al-rich inclusions. *Earth Planet. Sc. Lett.* **403**, 317-327.

Ludwig K. R. (2003) User's Manual for Isoplot 3.00. Berkeley Geochronology Center Special Publication No. 4, Berkeley, CA, 70pp.

McCoy T. J., Keil K., Scott E. R. D. and Haack H. (1993) Genesis of the IIICD iron meteorites: evidence from silicate-bearing inclusions. Meteoritics 28, 552–560.

Mughabghab S. F. (2003) Thermal neutron capture cross sections, resonance integrals, and G-factors. International Nuclear Data Committee INDC(NDS)-440 Distr. PG+R.

Nier A. O. (1950) A redetermination of the relative abundances of the isotopes of carbon, nitrogen, oxygen, argon, and potassium. *Phys. Rev.* **77**, 789–793.

Pilski A. S., Wasson J. T., Muszyński A., Kryza R., Karwowski Ł., and Nowak M. (2013) Low-Ir IAB irons from Morasko and other locations in central Europe: One fall, possibly distinct from IAB-MG. *Meteorit. Planet. Sci.* **48**, 2531-2541.

Qin L., Dauphas N, Wadhwa M., Markowski A., Gallino R., Janney P.E., and Bouman C. (2008) Tungsten nuclear anomalies in planetesimal cores. *Astrophys. J.* **674**, 1234–1241.

Qin L., Dauphas N., Horan M. F., Leya I., and Carlson R. W. (2015) Correlated cosmogenic W and Os isotopic variations in Carbo and implications for Hf-W chronology. *Geochim. Cosmochim. Acta* **153**, 91-104.

Rasmussen K.L. (1989) Cooling rates and parent bodies of iron meteorites from group IIICD, IAB, and IVB. *Physica Scripta* **39**, 410-416.

Touboul M. and Walker R. J. (2012) High precision tungsten isotope measurement by thermal ionization mass spectrometry. *Int. J. Mass Spectrom.* **309**, 109-117.

Vockenhuber C., Oberli F., Bichler M., Ahmad I., Quitté G., Meier M., Halliday A. N., Lee D.C., Kutschera W., Steier P., Gehrke R. J., and Helmer R. G. (2004) New half-life measurement of $^{182}$Hf: improved chronometer for the early solar system. *Phys. Rev. Lett.* **93** (172501).

Walker R. J. (2012) Evidence for homogeneous distribution of osmium in the protosolar nebula. *Earth Planet. Sc. Lett.* **351**, 36-44.

Wasson J. T. and Kallemeyn G. W. (2002) The IAB iron-meteorite complex: A group, five subgroups, numerous grouplets, closely related, mainly formed by crystal segregation in rapidly cooling melts. *Geochim. Cosmochim. Acta* **66**, 2445-2473.

Wittig N., Humayun M., Brandon A. D., Huang S., and Leya I. (2013) Coupled W-Os-Pt isotope systematics in IVB iron meteorites: In situ neutron dosimetry for W isotope chronology. *Earth Planet. Sci. Lett.* **361**, 152-161.

Worsham E. A., Bermingham K. R., and Walker R. J. (2016a) Siderophile element systematics of IAB complex iron meteorites: New insights into the formation of an enigmatic group. *Geochim. Cosmochim. Acta* **188**, 261-283.

Worsham E. A., Walker R. J., and Bermingham K. R. (2016b) High-precision molybdenum isotope analysis by negative thermal ionization mass spectrometry. *Int. J. Mass Spectrom. 407, 51-61.*